Research Square

Preprints are preliminary reports that have not undergone peer review.
They should not be considered conclusive, used to inform clinical practice,
or referenced by the media as validated information.

Mn site distribution and short-range magnetic order in the ludwigite Co2.19Mn0.81 11BO5: neutron diffraction and EPR study

Dina Fazlizhanova

dina.fazlik@gmail.com

National University of Science and Technology

Ivan Yatsyk

Kazan E. K. Zavoisky Physical-Technical Institute

Evgeniya Moshkina

Institute of Physics

Alexander Kurbakov

Petersburg Nuclear Physics Institute

Anna Susloparova

Petersburg Nuclear Physics Institute

Arina Nikitina

Kazan Federal University

Rushana Eremina

Kazan E. K. Zavoisky Physical-Technical Institute

Research Article

Keywords: Ludwigite, Cation distribution, Neutron diffraction, Electron paramagnetic resonance, Spin glass, Low-dimensional magnetism

Posted Date: November 20th, 2026

DOI: https://doi.org/10.21203/rs.3.rs-11693408/v1

License: This work is licensed under a Creative Commons Attribution 4.0 International License.
Read Full License

Additional Declarations: No competing interests reported.

Mn site distribution and short-range magnetic order in the ludwigite $Co_{2.19}Mn_{0.81}{}^{11}BO_5$: neutron diffraction and EPR study

D. I. Fazlizhanova[1,2*], I. V. Yatsyk[2], E. M. Moshkina[3], A. I. Kurbakov[4], A. E. Susloparova[4], A. D. Nikitina[6], S. S. Agafonov[5], R. M. Eremina[2]

[1]National University of Science and Technology "MISIS", Leninsky pr. 4, Moscow, 119049, Russia.
[2]Zavoisky Physical-Technical Institute, Federal Research Center "Kazan Scientific Center of RAS", Sibirsky tract 10/7, Kazan, 420029, Russia.
[3]Kirensky Institute of Physics, Federal Research Center KSC SB RAS, Akademgorodok 50, Krasnoyarsk, 660036, Russia.
[4]NRC Kurchatov Institute – PNPI, Gatchina, 188300, Russia.
[5]Kurchatov Institute (National Research Centre), Moscow, 123182, Russia.
[6]Kazan (Volga Region) Federal University, Kazan, 420008,Russia.

Contributing authors: dina.fazlik@gmail.com;

Abstract

Ludwigite oxyborates combine mixed valence, cation disorder and three-leg ladders of metal ions, which makes them model systems for frustrated low-dimensional magnetism. In most Mn-substituted crystals of Co_3BO_5, the ferrimagnetic order of the parent compound gives way to a spin glass. We combine neutron powder diffraction and X-band electron paramagnetic resonance (EPR) to follow how magnetic correlations develop on cooling in $Co_{2.19}Mn_{0.81}{}^{11}BO_5$. Because the neutron scattering lengths of Co and Mn have opposite signs, the diffraction data determine the cation distribution directly. Mn prefers the M4 site, which hosts Co^{3+} in the parent compound, and occupies it about twice as strongly as the other metal sites. Above 110 K the Co and Mn spins give a single collective EPR line with a g-factor intermediate between those of the two ions. Its intensity passes through a broad maximum near 170 K, which points to quasi-one-dimensional antiferromagnetic correlations along the ladders. Below

110 K a broad resonance centred at zero field appears, which we attribute to magnetically correlated regions that form far above the spin-glass freezing temperature. These regions do not develop long-range order. At 6.4 K the neutron pattern shows no magnetic Bragg peaks, only diffuse scattering from short-range magnetic correlations.

Keywords: Ludwigite, Cation distribution, Neutron diffraction, Electron paramagnetic resonance, Spin glass, Low-dimensional magnetism

1 Introduction

Ludwigites are oxyborates with the general formula $M_2^{2+}M^{3+}BO_5$, where M^{2+} and M^{3+} are divalent and trivalent metal cations, usually transition metals. Most ludwigites crystallize in the orthorhombic space group *Pbam* where metal cations occupy four nonequivalent octahedral sites, M1–M4. The MO_6 octahedra share edges and corners and form two kinds of three-leg ladders built from the 3-1-3 and 4-2-4 triads (Fig. 1) [1]. Mixed valence, cation disorder and these low-dimensional units lead to strong electronic correlations and competing exchange interactions. As a result, ludwigites show magnetic ground states ranging from long-range ferrimagnetic or antiferromagnetic order to spin-glass states [2]. The homometallic ludwigites Fe_3BO_5 and Co_3BO_5, which contain a single transition element in two valence states, are the reference compounds for studying how substitution changes these ground states.

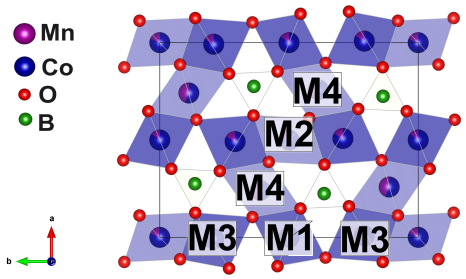

Fig. 1 Crystal structure of $Co_{2.19}Mn_{0.81}{}^{11}BO_5$ (space group *Pbam*) viewed along the *c* axis, showing the metal sites M1–M4, the BO_3 triangles and the 3-1-3 and 4-2-4 triads. Drawn with VESTA [3]

Magnetization measurements on single crystals of Co_3BO_5, Co^{2+} revealed anomalies at 17 and 45 K [4] and a pronounced magnetic anisotropy [5]. Neutron powder diffraction showed that Co_3BO_5 orders ferrimagnetically below $T_N = 42$ K with the propagation vector $\mathbf{k} = 0$ and the moments nearly parallel to the *b* axis [6]. The Co ions on the M4 site carry only about 0.5 μ_B, which identifies them as low-spin Co^{3+}

($S = 0$), while M1–M3 host high-spin Co^{2+} [6]. On heating, the M4 ions undergo a spin-state crossover [1, 7].

Replacing part of the Co by Mn changes both the balance of valence states and the network of exchange interactions, and the effect on the magnetic ground state is striking. Co_3BO_5 orders ferrimagnetically, but most Mn-substituted crystals studied so far never reach long-range order and freeze into a spin glass instead. Remarkably, the freezing temperature hardly depends on the Mn content and stays close to T_N of the parent compound: about 41 K in $Co_{1.7}Mn_{1.3}BO_5$ [8], 43 K in $Co_{2.25}Mn_{0.75}BO_5$ [9] and 44.5 K in $Co_{1.83}Mn_{1.17}BO_5$ [10]. A spin glass forms even in $Co_{1.46}Mn_{1.54}BO_5$, where the cations are almost perfectly ordered; there the freezing at 31.9 K has been attributed to competing exchange interactions within the 4-2-4 ladder rather than to cation disorder [11]. Yet $Co_{1.61}Mn_{1.39}BO_5$ has been reported to order ferrimagnetically at 60.8 K [10]. The magnetic state of these compounds is thus finely balanced, and understanding it requires knowing where the Mn ions sit.

The Mn distribution has so far been studied by single-crystal X-ray diffraction. It showed that in $Co_{1.7}Mn_{1.3}BO_5$ Mn prefers the M4 site, which holds about 65% Mn, while M1–M3 hold about 30% each [8]. Bond-valence sums for the same crystal gave an average Mn valence of +2.65, i.e., comparable amounts of Mn^{2+} and Mn^{3+} [8]. In $Co_{1.46}Mn_{1.54}BO_5$, grown from a borax-based flux, Mn occupies only the M2 and M4 sites [11].

X-ray diffraction distinguishes Co ($Z = 27$) and Mn ($Z = 25$) only weakly, so site occupancies derived from X-ray data rest on a small scattering contrast. Neutron diffraction provides a much larger contrast: the coherent scattering lengths of Co (2.49 fm) and Mn (−3.73 fm) differ in sign [12]. To our knowledge, no neutron diffraction data have been reported for Co-rich $Co_{3-x}Mn_xBO_5$.

Here we report neutron powder diffraction at room temperature and at 6.4 K, together with X-band EPR, on $Co_{2.19}Mn_{0.81}{}^{11}BO_5$. The neutron data confirm the non-random distribution of Mn found by X-ray diffraction, show that no long-range magnetic order develops down to 6.4 K, and reveal short-range magnetic correlations. The EPR spectra show how these correlations develop on cooling, from quasi-one-dimensional correlations along the ladders to the formation of correlated regions well above the spin-glass freezing.

2 Samples and Experimental Details

2.1 Synthesis

Crystals of $Co_{3-x}Mn_x{}^{11}BO_5$ were grown by the flux method from a $Bi_2Mo_3O_{12}$-based solvent diluted with Na_2CO_3. To reduce neutron absorption, ^{11}B-enriched boric acid, $H_3{}^{11}BO_3$, was used. The flux system $Bi_2Mo_3O_{12}$: 1.88 $H_3{}^{11}BO_3$: 0.7 Na_2O : 0.23 Mn_2O_3 : 0.23 Co_2O_3 : 1.85 CoO (molar ratio) was melted in air at 1100 °C in a 100 cm^3 platinum crucible in a resistive furnace. The boric acid was added first, in small portions, since it decomposes into $^{11}B_2O_3$ and water vapour. A mixture of Bi_2O_3 and MoO_3 followed, then Na_2CO_3, which decomposes into Na_2O and CO_2, and finally the Mn_2O_3 and Co_2O_3 powders, each in portions. The melt was homogenized at 1100 °C for 3 h. Its saturation temperature was 970 °C, and the high-temperature

crystallizing phase consisted of black elongated prisms. Powder X-ray diffraction of these crystals showed a single orthorhombic ludwigite phase.

For the growth, the melt was again homogenized at 1100 °C for 3 h, cooled at 200 °C/h to 960 °C and then at 3 °C/day for 6 days. The crucible was then taken out of the furnace and the melt was decanted. The crystals, black elongated prisms, were separated from the flux residue by etching in a 20% aqueous solution of nitric acid. For the neutron and EPR measurements the crystals were ground to powder.

2.2 X-ray Fluorescence

The elemental composition and the spatial distribution of Co and Mn were determined by X-ray fluorescence (XRF) using a Bruker S8 Tiger spectrometer.

2.3 Neutron Diffraction

Neutron powder diffraction patterns were collected on the DISK multidetector diffractometer at the IR-8 research reactor (National Research Centre "Kurchatov Institute", Moscow) with a constant wavelength $\lambda = 2.438$ Å in the 2θ range 10–90°. Patterns were recorded at room temperature and at 6.4 K; for the low-temperature measurement the sample was mounted in a closed-cycle cryostat. The structure was refined by the Rietveld method with FullProf [13]. Owing to the ^{11}B enrichment, absorption by boron is small at this wavelength.

2.4 EPR

EPR spectra of powdered $Co_{2.19}Mn_{0.81}{}^{11}BO_5$ were recorded with a Bruker EMXplus X-band spectrometer at $\nu = 9.40$ GHz in the temperature range 10–298 K, using helium-flow cryostat.

3 Results and Discussion

3.1 Composition

The XRF elemental maps (Fig. 2) show a uniform distribution of Co and Mn across the sample. The dark spots appear at the same positions in the Co and Mn maps and therefore reflect the surface topography rather than a segregation of either element. The Co/Mn ratio is 2.70, which corresponds to $x = 0.81$ in $Co_{3-x}Mn_xBO_5$, i.e., $Co_{2.19}Mn_{0.81}BO_5$.

3.2 Crystal Structure and Cation Distribution

All reflections at both temperatures are indexed in space group *Pbam*. Figure 3 shows the Rietveld refinement of the 6.4 K pattern ($R_{wp} = 15.5\%$, $R_{exp} = 9.17\%$, $\chi^2 = 2.85$). The lattice parameters are listed in Table 1. On cooling from room temperature to 6.4 K the cell contracts anisotropically: a and c decrease by about 0.5%, whereas b decreases by only 0.09%.

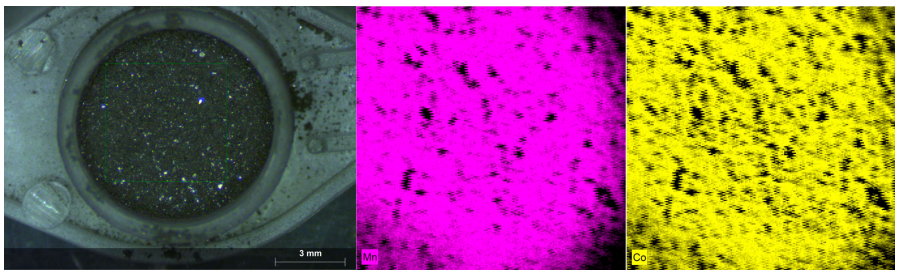

Fig. 2 Optical image of the sample (left) and XRF elemental maps of Mn (centre) and Co (right). Both elements are distributed uniformly; the dark spots coincide in the two maps and reflect the surface topography. Co/Mn = 2.70

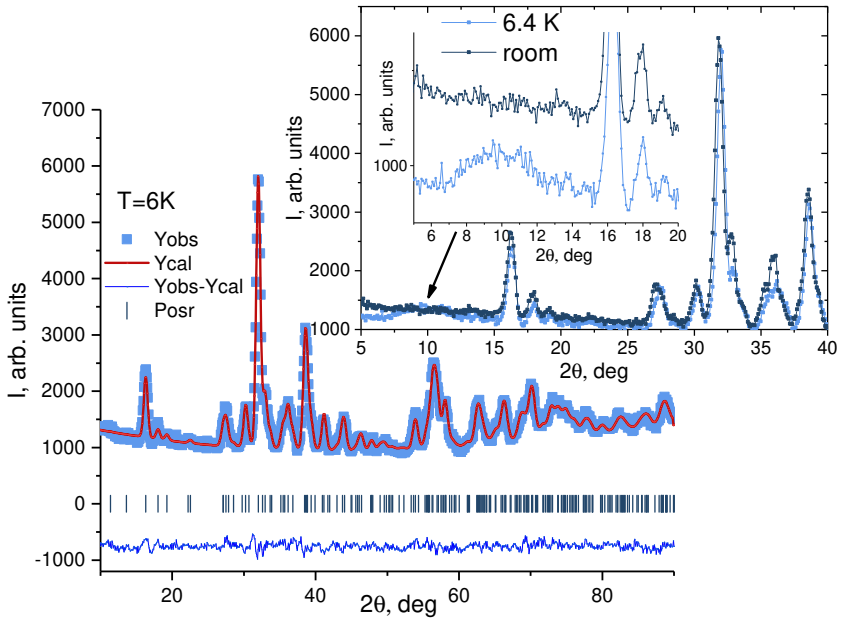

Fig. 3 Rietveld refinement of the neutron powder diffraction pattern of $Co_{2.19}Mn_{0.81}BO_5$ at 6.4 K (λ = 2.438 Å): observed (symbols) and calculated (line) intensities, their difference (bottom) and Bragg positions (ticks); R_{wp} = 15.5%, R_{exp} = 9.17%, χ^2 = 2.85. Inset: patterns at 6.4 K and room temperature. Inner inset: low-angle region, with the room-temperature data offset vertically for clarity; at room temperature the background is featureless, while at 6.4 K a broad diffuse maximum appears near $2\theta \approx 10°$

The occupancies refined from the 6.4 K pattern give the composition $Co_{2.18}Mn_{0.82}BO_5$ (Co/Mn = 2.66), in agreement with the XRF result (Co/Mn = 2.70). The atomic coordinates and site occupancies are listed in Table 2.

The Mn ions are distributed over the metal sites in a non-random way. The M1, M2 and M3 sites contain 19.6–21.2% Mn, whereas the M4 site contains 41.8% Mn, about twice as much.

Table 1 Lattice parameters of $Co_{2.19}Mn_{0.81}BO_5$ from neutron powder diffraction

T	a (Å)	b (Å)	c (Å)	V (Å^3)
Room temperature	9.3272(13)	12.3504(18)	3.0525(5)	351.63 (9)
6.4 K	9.2820(11)	12.3367(16)	3.0378(4)	347.85(8)

Table 2 Wyckoff positions, fractional atomic coordinates and site occupancies of $Co_{2.18}Mn_{0.82}BO_5$ refined from neutron powder diffraction at 6.4 K. The metal sites are labelled as in Fig. 1

Site	Wyckoff	x	y	z	Occ. Co	Occ. Mn
M1	2c	0.5	0	0	0.800(18)	0.200(18)
M2	2b	0	0	0.5	0.788(18)	0.212(18)
M3	4g	0.508(4)	0.289(4)	0	0.804(12)	0.196(12)
M4	4h	0.26(4)	0.11(3)	0.5	0.582(9)	0.418(9)
O1	4h	0.3735(9)	0.3631(16)	0.5		
O2	4h	0.3528(10)	−0.0450(8)	0.5		
O3	4g	0.1129(8)	0.0777(7)	0		
O4	4h	0.1584(10)	0.2681(7)	0.5		
O5	4g	0.3958(10)	0.1431(9)	0		
B	4h	0.2250(9)	0.3638(13)	0.5		

Table 3 compares this distribution with the single-crystal X-ray results for higher Mn contents. For $Co_{1.7}Mn_{1.3}BO_5$ [8] the pattern is the same as in our sample: M4 holds about twice the Mn fraction of each of the other sites, although the total Mn content is 1.6 times higher. The neutron data, with their much larger Co/Mn contrast, thus confirm the X-ray distribution and show that the ratio of the site occupancies is retained at lower Mn content. The nearly complete cation order in $Co_{1.46}Mn_{1.54}BO_5$ [11], with Mn only on M2 and M4, differs from both. That sample was grown from a borax-based flux, whereas $Co_{1.7}Mn_{1.3}BO_5$ [8] and our sample were grown from $Bi_2Mo_3O_{12}$-based fluxes, which suggests that the degree of cation order depends on the growth conditions. A similar sensitivity to the cation arrangement is known for the monoclinic ludwigite Cu_2FeBO_5: its crystals show cation disorder on several metal sites [14], and calculations show that the type of magnetic order depends strongly on how Fe is distributed over the sites [15].

Table 3 Mn fraction on each metal site of $Co_{3-x}Mn_xBO_5$ ($x \leq 1.54$). For a random distribution all four sites would have the same Mn fraction. The site labels of Refs. [8, 11] follow the same convention: M2–M4 is the edge-sharing triad with the shortest metal–metal distance

Composition	Method	T (K)	M1	M2	M3	M4
$Co_{2.18}Mn_{0.82}BO_5$ (this work)	neutron	6.4	0.20	0.21	0.20	0.42
$Co_{1.7}Mn_{1.3}BO_5$ [8]	X-ray	296	0.30	0.30	0.33	0.65
$Co_{1.46}Mn_{1.54}BO_5$ [11]	X-ray	150	0.08	1.00	0	1.00

In Co_3BO_5 the M4 site hosts the trivalent Co^{3+} ions [1, 6], so Mn preferentially substitutes Co on the site of the trivalent cation. The M4 site belongs to the 4-2-4 triad, in which the $M2O_6$ and $M4O_6$ octahedra share an edge and the M2–M4 distance, 2.77 Å at 6.4 K, is the shortest metal–metal distance in the structure. This value lies between 2.75 Å in Co_3BO_5 and 2.80 Å in $Co_{1.7}Mn_{1.3}BO_5$ [8]. Because M4 is the trivalent site of the parent compound, part of the Mn on M4 is likely trivalent, in line with the mixed Mn^{2+}/Mn^{3+} valence found for $Co_{1.7}Mn_{1.3}BO_5$ [8]. The diffraction data alone do not determine the Mn valence. For $Co_{2.25}Mn_{0.75}BO_5$, the effective moment, 8.72 μ_B per formula unit, is slightly larger than the 8.55 μ_B expected if all Mn is divalent and Co^{3+} is low-spin [9]. Replacing part of the low-spin Co^{3+} on M4 by Mn^{3+}, with a corresponding increase in Co^{2+}, raises the expected moment, so these data are compatible with a partial Mn^{3+} substitution on M4, although the difference is small.

3.3 Magnetic State at 6.4 K

Magnetization measurements on $Co_{2.25}Mn_{0.75}BO_5$, a sample of very similar composition grown by the same procedure, show a spin-glass transition at $T_g = 43$ K [9].

The inset of Fig. 3 compares the patterns collected at room temperature and at 6.4 K, well below T_g. At 6.4 K neither new reflections nor additional intensity on the nuclear reflections appear. Hence, no long-range magnetic order is present within the sensitivity of the experiment. In Co_3BO_5, by contrast, magnetic Bragg peaks with $\mathbf{k} = 0$ appear below $T_N = 42$ K [6].

The two patterns differ at low scattering angles (inner inset of Fig. 3). At room temperature the low-angle background is smooth and featureless, as expected for paramagnetic scattering. At 6.4 K a broad diffuse maximum appears near $2\theta \approx 10°$, which corresponds to a scattering vector $Q = 4\pi \sin\theta/\lambda \approx 0.45$ Å^{-1}. Such diffuse scattering is the signature of short-range magnetic correlations. In Co_3BO_5 magnetic diffuse scattering is observed above T_N and gives way to magnetic Bragg peaks below it [6]; here it persists far below T_g. The frozen state of $Co_{2.19}Mn_{0.81}BO_5$ therefore has only short-range magnetic order, as expected for a spin glass. Spin-glass states have also been reported for $Co_{1.83}Mn_{1.17}BO_5$ [10] and $Co_{1.7}Mn_{1.3}BO_5$ [8].

3.4 EPR

3.4.1 Spectra and Line-Shape Analysis

Figures 4 and 5 show the EPR spectra of $Co_{2.19}Mn_{0.81}{}^{11}BO_5$ between 10 and 50 K and between 70 and 186 K. The spectra of $Co_{2.25}Mn_{0.75}BO_5$ at higher temperatures, between 290 and 700 K, were reported earlier [16].

Above about 110 K the spectrum consists of a single broad line. Its linewidth is comparable to its resonance field, so the resonance at negative field, i.e., the absorption of the counter-rotating circular component of the microwave field, also contributes to the signal near zero field. Each line was therefore described by an asymmetric

Lorentzian that includes the resonances at both $+H_{\rm res}$ and $-H_{\rm res}$ [17, 18]:

$$\frac{dP}{dH} = \frac{d}{dH}\left(\frac{\Delta H + \alpha(H - H_{\rm res})}{(H - H_{\rm res})^2 + \Delta H^2} + \frac{\Delta H - \alpha(H + H_{\rm res})}{(H + H_{\rm res})^2 + \Delta H^2}\right), \tag{1}$$

where $H_{\rm res}$ is the resonance field, ΔH is the linewidth and α is the asymmetry parameter, i.e., the admixture of dispersion to absorption. The integrated intensity of each line was calculated from its fit parameters.

Below 110 K the spectrum is more complex, and four lines are needed to describe it:

1. a line centred at zero magnetic field with a linewidth of about 500 Oe, which is a background signal of the resonator
2. a much broader line, about 2000 Oe linewide, also centred at zero megnetic field, which we attribute to magnetically correlated regions of the sample (Sect. 3.4.3);
3. the main line, which continues the single line observed above 110 K;
4. a weak narrow line at $g \approx 1.97$, which we attribute to isolated paramagnetic centres of manganese.

Figure 6 shows the temperature dependence of the integrated intensity, linewidth and resonance field of the main EPR line.

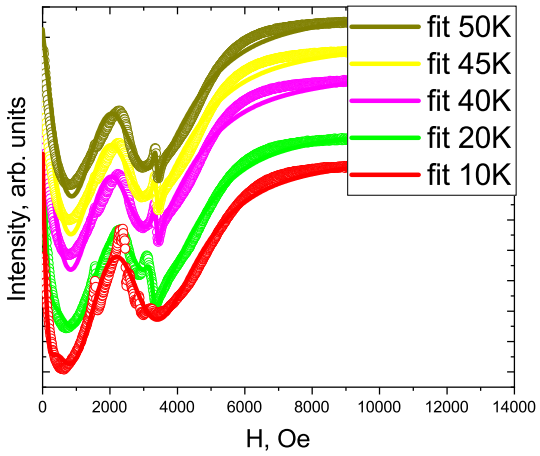

Fig. 4 EPR spectra of $Co_{2.19}Mn_{0.81}{}^{11}BO_5$ between 10 and 50 K. Symbols: experiment; lines: fit with four components of the form of Eq. (1)

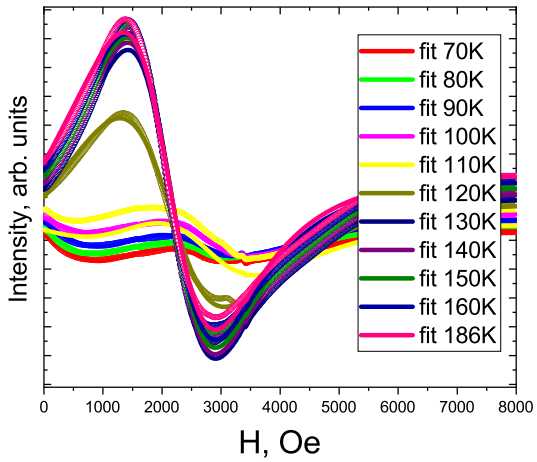

Fig. 5 EPR spectra of $Co_{2.19}Mn_{0.81}{}^{11}BO_5$ between 70 and 186 K. Symbols: experiment; lines: fit with Eq. (1)

3.4.2 The Main EPR Line: Collective Resonance of Co and Mn Spins

Above 120 K the resonance field of the main line is constant, $H_{\mathrm{res}} = 2150$ Oe, which corresponds to

$$g = \frac{h\nu}{\mu_{\mathrm{B}} H_{\mathrm{res}}} = 3.12 \pm 0.01. \tag{2}$$

This g-factor does not belong to either of the magnetic ions on its own. Mn^{2+} ($S = 5/2$) in an octahedral oxygen environment has g slightly below 2 [19], and EPR of manganese ions is observed over a wide temperature range, from 4.2 K to above 800 K [20]. High-spin Co^{2+} ($S = 3/2$) in an octahedral environment has a ground Kramers doublet with an spin $S = 3/2$ and $g \approx 4.1$–4.3 [19, 21]; because of its fast spin–lattice relaxation, its EPR is usually observed only below about 100 K [21]. Low-spin Co^{3+} ($S = 0$) gives no EPR signal. If Co^{2+} and Mn^{2+} resonated independently, we would therefore expect a Mn^{2+} line near $g = 2$ at all temperatures and a Co^{2+} line near $g = 4.2$ below 100 K. Instead, a single line with an intermediate g-factor is observed up to room temperature.

This is the signature of a collective resonance of exchange-coupled ions [22]. When the exchange interaction between the Co and Mn spins is much stronger than the difference of their Zeeman energies, the two spin systems precess together, and a single line appears at the averaged g-factor

$$g_{\mathrm{eff}} = \frac{\chi_{\mathrm{Co}}\, g_{\mathrm{Co}} + \chi_{\mathrm{Mn}}\, g_{\mathrm{Mn}}}{\chi_{\mathrm{Co}} + \chi_{\mathrm{Mn}}}, \tag{3}$$

where χ_{Co} and χ_{Mn} are the static susceptibilities of the coupled Co and Mn spins. With $g_{\mathrm{Co}} \approx 4.2$ and $g_{\mathrm{Mn}} \approx 2.0$, the measured $g = 3.12$ implies that Co and Mn contribute roughly equally to the susceptibility of the resonating spins. Similar collective resonances were observed in $Mn_{2.25}Co_{0.75}BO_5$ [23], in Mn-doped $La_{2-x}Sr_xCuO_{4+\delta}$ [22] and in the spin-Peierls magnet $Cu_{1-x}Ni_xGeO_3$ [24].

The fast relaxation of Co^{2+} also determines which spins contribute to the EPR line. Co^{2+} ions take part in the collective mode through their exchange coupling to Mn, whereas Co^{2+} ions in a purely Co environment relax too fast to give an observable signal at these temperatures. The main line is therefore dominated by Mn-containing units of the structure, such as Co–Mn–Co triads, and its intensity reflects the susceptibility of these units rather than that of all spins in the sample.

3.4.3 Onset of Magnetic Correlations at 110 K

All three parameters of the main line change abruptly at about 110 K (Fig. 6). On cooling through this temperature, the linewidth and the resonance field pass through a sharp peak, and the intensity drops steeply. At the same time the spectrum changes its shape, and the broad line centered at zero magnetic field appears. Between 100 and 40 K the intensity of the main line decreases only slowly on further cooling.

We interpret these observations as follows. Below 110 K, magnetically correlated regions start to form in the sample. Spins in these regions experience strong internal fields and no longer contribute to the paramagnetic main line; instead, they give the broad resonance centred at zero magnetic field. On cooling, the correlated regions grow at the expense of the paramagnetic part of the sample and finally freeze into the spin-glass state, which sets in at $T_{\mathrm{g}} = 43$ K in $Co_{2.25}Mn_{0.75}BO_5$ [9]. The diffuse magnetic scattering observed at 6.4 K (Sect. 3.3) reflects the short-range order of these frozen regions. The anomaly at 110 K thus marks the onset of magnetic correlations far above the freezing temperature. No anomaly near 110 K has been reported in the static susceptibility of $Co_{2.25}Mn_{0.75}BO_5$ [9], which suggests that only a fraction of the spins is involved at this temperature.

3.4.4 Intensity Maximum and Low-Dimensional Correlations

Above 110 K the intensity of the main line continues to increase on heating and passes through a broad maximum at about 170 K (Fig. 6a). For non-interacting spins the intensity would follow the Curie law and decrease monotonically with increasing temperature. A broad maximum well above any ordering or freezing temperature is instead characteristic of low-dimensional antiferromagnets. In chains and ladders, short-range antiferromagnetic correlations reduce the susceptibility already at temperatures comparable to the exchange energy along the chain, which produces the broad maximum first calculated by Bonner and Fisher [25]. The maximum lies about four times above T_{g}, as expected when the exchange along the ladders is much stronger than the coupling between them.

The static susceptibility of $Co_{2.25}Mn_{0.75}BO_5$ shows no such maximum and increases monotonically on cooling down to T_{g} [9]. The two results do not contradict each other. The static susceptibility sums the contributions of all spins, and even a small contribution of weakly correlated or uncompensated spins is enough to mask a

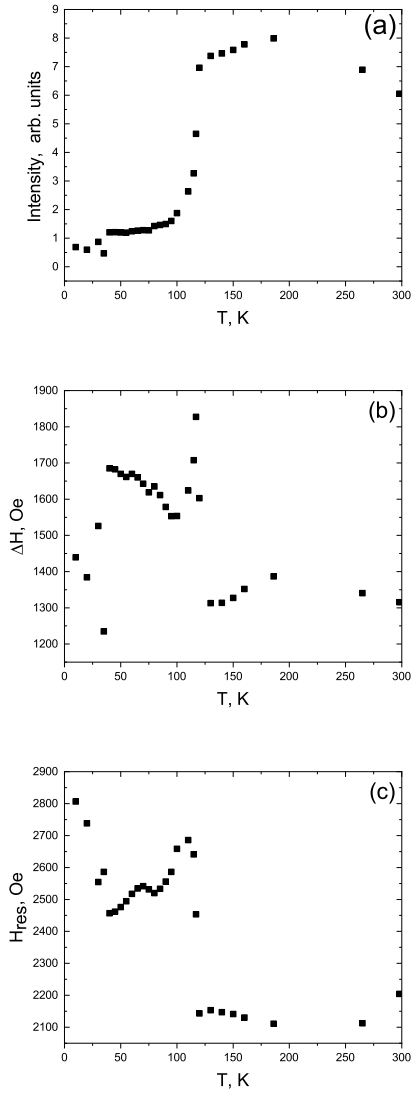

Fig. 6 Temperature dependence of (a) the integrated intensity, (b) the linewidth and (c) the resonance field of the main EPR line of $Co_{2.19}Mn_{0.81}{}^{11}BO_5$

broad maximum. The EPR line, by contrast, is dominated by the Mn-containing units (Sect. 3.4.2). We therefore attribute the intensity maximum to quasi-one-dimensional antiferromagnetic correlations along the three-leg ladders, in which the Co–Mn–Co triads are coupled to neighbouring triads of different composition.

4 Conclusions

We combined neutron powder diffraction and X-band EPR to study the Mn-substituted ludwigite $Co_{2.19}Mn_{0.81}{}^{11}BO_5$.

The neutron data, with their large Co/Mn scattering contrast, show that Mn replaces Co non-randomly. The M4 site, which hosts low-spin Co^{3+} in Co_3BO_5, contains about twice as much Mn as each of the other three metal sites. The same ratio was found by X-ray diffraction for $Co_{1.7}Mn_{1.3}BO_5$, so this site preference persists over a wide composition range.

No long-range magnetic order develops down to 6.4 K, well below the spin-glass freezing temperature of a compound of similar composition. Instead, diffuse scattering shows that the frozen state has only short-range magnetic order.

The EPR spectra show how these correlations develop on cooling. Above 110 K, Co and Mn spins resonate as a single exchange-coupled mode with $g = 3.12$. Its intensity passes through a broad maximum near 170 K, which indicates quasi-one-dimensional antiferromagnetic correlations along the three-leg ladders. Below 110 K, magnetically correlated regions begin to form; they grow on cooling and finally freeze into the spin-glass state.

Because the M4 site is non-magnetic in Co_3BO_5, its partial occupation by Mn introduces magnetic moments and exchange paths that are absent in the parent compound. A systematic neutron study across the $Co_{3-x}Mn_xBO_5$ series would show whether the occupation of this site controls the balance between ferrimagnetic order and spin-glass freezing.

Acknowledgements. The work was carried out using the equipment of the unique scientific installation "Neutron Research Complex based on the IR-8 Reactor".This work was supported by the Russian Science Foundation (project no. 23-72-00047)

Declarations

- **Competing interests**: The authors have no relevant financial or non-financial interests to disclose.
- **Data availability**: The data that support the findings of this study are available from the corresponding author upon request.

References

[1] Kazak, N.V., Platunov, M.S., Knyazev, Y.V., Molokeev, M.S., Gorev, M.V., Ovchinnikov, S.G., Pchelkina, Z.V., Gapontsev, V.V., Streltsov, S.V., Bartolomé, J., Arauzo, A., Yumashev, V.V., Gavrilkin, S.Y., Wilhelm, F., Rogalev, A.: Spin state crossover in Co_3BO_5. Phys. Rev. B **103**, 094445 (2021) https://doi.org/10.1103/PhysRevB.103.094445

[2] Continentino, M.A., Fernandes, J.C., Guimarães, R.B., Boechat, B., Saguia, A.: Magnetism in highly anisotropic borates: experiment and theory. In: Narlikar, A.V. (ed.) Frontiers in Magnetic Materials, pp. 385–413. Springer, Berlin (2005). https://doi.org/10.1007/3-540-27284-4_14

[3] Momma, K., Izumi, F.: VESTA 3 for three-dimensional visualization of crystal, volumetric and morphology data. J. Appl. Crystallogr. **44**, 1272 (2011) https://doi.org/10.1107/S0021889811038970

[4] Ivanova, N.B., Vasil'ev, A.D., Velikanov, D.A., Kazak, N.V., Ovchinnikov, S.G., Petrakovskii, G.A., Rudenko, V.V.: Magnetic and electrical properties of cobalt oxyborate Co_3BO_5. Phys. Solid State **49**, 651 (2007) https://doi.org/10.1134/S1063783407040087

[5] Freitas, D.C., Continentino, M.A., Guimarães, R.B., Fernandes, J.C., Ellena, J., Ghivelder, L.: Structure and magnetism of homometallic ludwigites: $Co_3O_2BO_3$ versus $Fe_3O_2BO_3$. Phys. Rev. B **77**, 184422 (2008) https://doi.org/10.1103/PhysRevB.77.184422

[6] Freitas, D.C., Medrano, C.P.C., Sanchez, D.R., Nuñez Regueiro, M., Rodríguez-Velamazán, J.A., Continentino, M.A.: Magnetism and charge order in the ladder compound $Co_3O_2BO_3$. Phys. Rev. B **94**, 174409 (2016) https://doi.org/10.1103/PhysRevB.94.174409

[7] Galdino, C.W., Freitas, D.C., Medrano, C.P.C., Tartaglia, R., Rigitano, D., Oliveira, J.F., Mendonça, A.A., Ghivelder, L., Continentino, M.A., Sanchez, D.R., Granado, E.: Magnetic, electronic, structural, and thermal properties of the $Co_3O_2BO_3$ ludwigite in the paramagnetic state. Phys. Rev. B **100**, 165138 (2019) https://doi.org/10.1103/PhysRevB.100.165138

[8] Knyazev, Y.V., Ivanova, N.B., Kazak, N.V., Platunov, M.S., Bezmaternykh, L.N., Velikanov, D.A., Vasiliev, A.D., Ovchinnikov, S.G., Yurkin, G.Y.: Crystal structure and magnetic properties of Mn substituted ludwigite $Co_3O_2BO_3$. J. Magn. Magn. Mater. **324**, 923 (2012) https://doi.org/10.1016/j.jmmm.2011.07.044

[9] Popov, D., Shustov, V., Batulin, R., Cherosov, M., Moshkina, E., Eremina, R.: Spin-glass transition in $Mn_{0.75}Co_{2.25}BO_5$ compound. J. Supercond. Nov. Magn. **38**, 152 (2025)

[10] Popov, D.V., Gavrilova, T.P., Cherosov, M.A., Shustov, V.A., Moshkina, E.M., Fazlizhanov, I.I., Eremina, R.M.: Magnetism and specific heat of ludwigites $Mn_{1.17}Co_{1.83}BO_5$ and $Mn_{1.39}Co_{1.61}BO_5$. J. Alloys Compd. **976**, 173143 (2024) https://doi.org/10.1016/j.jallcom.2023.173143

[11] Heringer, M.A.V., Mariano, D.L., Freitas, D.C., Baggio-Saitovitch, E., Continentino, M.A., Sanchez, D.R.: Spin-glass behavior in $Co_3Mn_3(O_2BO_3)_2$ ludwigite with weak disorder. Phys. Rev. Mater. **4**, 064412 (2020) https://doi.org/10.1103/PhysRevMaterials.4.064412

[12] Sears, V.F.: Neutron scattering lengths and cross sections. Neutron News **3**, 26 (1992) https://doi.org/10.1080/10448639208218770

[13] Rodríguez-Carvajal, J.: Recent advances in magnetic structure determination by neutron powder diffraction. Physica B **192**, 55 (1993) https://doi.org/10.1016/0921-4526(93)90108-I

[14] Gokhfeld, Y.S., Kazak, N.V., Bel'skaya, N.A., Molokeev, M.S., Gudim, I.A., Kondratiev, O.A., Eremin, E.V., Knyazev, Y.V., Velikanov, D.A., Ovchinnikov, S.G.: Structural disorder, specific heat, and magnetic transitions in Cu_2FeBO_5. J. Exp. Theor. Phys. **137**, 494 (2023)

[15] Nazarenko, I.I., Sofronova, S.N., Moshkina, E.M.: Magnetic ordering dependence on iron ions distribution in Cu_2FeBO_5 ludwigite. J. Exp. Theor. Phys. **126**, 674 (2018) https://doi.org/10.1134/S1063776118050047

[16] Muftakhutdinov, A.R., Popov, D.V., Fazlizhanov, I.I., Likerov, R.F., Makarchenko, A.S., Ganeeva, Y.M., Moshkina, E.M., Eremina, R.M.: High-temperature properties of $Mn_{0.75}Co_{2.25}BO_5$ compound. Magn. Reson. Solids **26**, 24301 (2024) https://doi.org/10.26907/mrsej-24301

[17] Popov, D.V., Batulin, R.G., Cherosov, M.A., Yatsyk, I.V., Yanilkin, I.V., Moshkina, E.M., Gubaidullin, A.T., Fazlizhanova, D.I., Eremina, R.M.: Spin crossover in magnetic field for Cu_2MnBO_5:Cr. J. Alloys Compd. **1040**, 183213 (2025) https://doi.org/10.1016/j.jallcom.2025.183213

[18] Joshi, J.P., Bhat, S.V.: On the analysis of broad Dysonian electron paramagnetic resonance spectra. J. Magn. Reson. **168**, 284 (2004) https://doi.org/10.1016/j.jmr.2004.03.018

[19] Abragam, A., Bleaney, B.: Electron Paramagnetic Resonance of Transition Ions. Clarendon Press, Oxford (1970)

[20] Yatsyk, I., Eremina, R., Shakirzyanov, M., Mukovskii, Y., Krug von Nidda, H.-A., Loidl, A.: Abrupt changes in the temperature dependence of the ESR linewidth of $La_{1-x}Ca_xMnO_3$ single crystals. JETP Lett. **87**, 447 (2008)

[21] Shapovalov, V.V., Shapovalov, V.A., Drokina, T.V., Vorotynov, A.M., Val'kov, V.I.: Distribution of cobalt Co^{2+} ions in single crystals of spinel $Li_{0.5}Ga_{2.5}O_4$. Phys. Met. Metallogr. **125**, 27 (2024) https://doi.org/10.1134/S0031918X23602883

[22] Kochelaev, B., Kan, L., Elschner, B., Elschner, S.: Spin dynamics in $La_{2-x}Sr_xCuO_{4+\delta}$ doped with Mn as revealed by an ESR study. Phys. Rev. B **49**, 13106 (1994) https://doi.org/10.1103/PhysRevB.49.13106

[23] Eremina, R., Moshkina, E., Yatsyk, I., Shustov, V.: Crystal structure and EPR spectra of $Mn_{2.25}Co_{0.75}BO_5$. Bull. Russ. Acad. Sci. Phys. **88**, 1126 (2024)

[24] Glazkov, V., Smirnov, A., Eremina, R., Dhalenne, G., Revcolevschi, A.: Magnetic

resonance of spin clusters and triplet excitations in a spin-Peierls magnet with impurities. J. Exp. Theor. Phys. **93**, 143 (2001)

[25] Bonner, J.C., Fisher, M.E.: Linear magnetic chains with anisotropic coupling. Phys. Rev. **135**, 640 (1964) https://doi.org/10.1103/PhysRev.135.A640